

**QUANTIFICATION OF OLEORESIN IN AGARWOOD BY MEANS OF
MICRO-COMPUTED TOMOGRAPHY AND DIGITAL IMAGE PROCESSING**

by

KHAIR'IAH BINTI YAZID @ KHALID

**Thesis submitted in fulfillment of the requirements
for the degree of
Master of Science**

MAY2011

ACKNOWLEDGEMENTS

Praise to Allah Most High, Gracious and Mercy, this thesis would not have been completed without His will, infinite guidance and cherishing care. I would like to express my deepest thanks to my family. I am really grateful for all the love and support they always provided.

I would like to acknowledge the efforts of my main supervisor Prof. Mohd. Zaid Abdullah. The help and guidance he provided for me throughout my study are deeply appreciated. I would like to extend my thanks to Dr Mohd Ashhar Khalid and Dr. Abdul Aziz Mohamed for giving me encouragement and assistance. I am grateful of all the help and support they always provided.

Special thanks to Datuk Dr Daud Mohamad, general director of the Malaysian Nuclear Agency and Computed Tomography Laboratory group for allowing us to perform the CT scans of the agarwood. I also thank Dr Mat Rasol Awang, Agro Technology and Biosciences Division of the Malaysian Nuclear Agency for providing agarwood samples.

TABLE OF CONTENTS

	Page
ACKNOWLEDGEMENTS	ii
TABLE OF CONTENTS	iii
LIST OF TABLES	vi
LIST OF FIGURES	vii
LIST OF SYMBOLS	xi
LIST OF ABBREVIATIONS	xiii
LIST OF PUBLICATIONS	xv
ABSTRAK	xvi
ABSTRACT	xviii
CHAPTER 1 INTRODUCTION	
1.1 Introduction	1
1.2 Problem Statement	2
1.3 Objective	4
1.4 Scope of research	4
1.5 Thesis Outline	4
CHAPTER 2 LITERATURE SURVEY	
2.1 Introduction	6
2.2 Revolution and Recent Development in High Resolution CT Systems	6
2.3 Application of micro-CT	10
2.4 Application of micro-CT in wood research	12
2.5 Image processing in wood imaging	14
CHAPTER 3 THEORY	
3.1 Introduction	16
3.2 Type of CT systems	19
3.3 Image Reconstruction	20
3.4 Projection geometry and system geometry	22
3.5 Projection and line integral	25

3.6	Radon transform	28
3.7	Analytical algorithm	29
	3.7.1 Back-projection	29
	3.7.2 Central slice theorem	32
	3.7.3 Filtered back-projection principle	34
	3.7.4 Filtered back-projection algorithm	37
3.8	Filters for FBP	38
3.9	Fan-beam	41
	3.9.1 Equi-angular rays	43
	3.9.2 Equal-spaced rays	45
	3.9.3 Fan beam to parallel beam rebinning	46
3.10	Artifacts in CT	48
3.11	CT Image Display	50
3.12	Principle of image thresholding	52

CHAPTER 4 DATA ACQUISITION AND IMAGE RECONSTRUCTION SYSTEMS

4.1	Introduction	55
4.2	System Description	55
	4.2.1 Detector	58
	4.2.2 X-ray Source	60
	4.2.3 Rotation table	60
4.3	Software	62

CHAPTER 5 IMAGE RECONSTRUCTION USING XRECON

5.1	Introduction	63
5.2	XRecon	63
5.3	Experimental Work	68
	5.3.1 Phantoms	68

5.3.2	CT scanning	70
5.3.3	Reconstruction process	71
5.4	Results and Discussion	72
CHAPTER 6 QUANTIFICATION OF OLEORESIN IN CT IMAGE		
6.1	Introduction	83
6.2	Oleoresin in Agarwood	83
6.3	Agarwood composition	86
6.4	Experimental Work	89
6.4.1	Simulation of quantification method using image threshold	89
6.4.2	Samples	91
6.4.3	Image Acquisition: Micro-CT	92
6.4.4	Reconstruction process	96
6.5	Results and Discussion	97
6.5.1	Simulation	97
6.5.2	Cross-section CT Image	99
6.5.3	Segmentation and Quantification	111
CHAPTER 7 CONCLUSION AND RECOMMENDATIONS		
7.1	The reconstruction software	121
7.2	Micro-CT application in agarwood	122
7.3	Computer aided quantification method	122
7.4	Recommendations	123
REFERENCES		125
APPENDIX A		132
APPENDIX B		140

LIST OF TABLES

		Page
Table 2.1	General classification of computed tomography (Ketcham & Carlson, 2001)	6
Table 3.1	Comparison between different tomography modalities	17
Table 3.2	Descriptions of each CT system geometry	20
Table 4.1	Parameters of the detector.	58
Table 5.1	Comparison XRecon with commercial reconstruction software	64
Table 6.1	Summarizes of the samples	92
Table 6.2	The details of the micro-CT scanner	93
Table 6.3	Results from software generated image	98
Table 6.4	Calculated values in CT image with XRecon	118
Table 7.1	The proposed grading system	124

LIST OF FIGURES

		Page
Figure 3.1	Attenuation diagram of Beer law.....	18
Figure 3.2	Geometry for each CT system (a) fan beam, (b) cone beam and (c) parallel beam	20
Figure 3.3	Data sampling pattern.	22
Figure 3.4	Projection geometry for each CT system (a) fan beam projection, (b) cone beam projection and (c) parallel beam projection	23
Figure 3.5	Illustration of distance between X-ray tube focal point and the system detector (<i>SDD</i>) over the (distance between the X-ray tube focal spot and the sample (<i>SOD</i>) in CT system.....	23
Figure 3.6	Comparison pixel versus voxel (a) 2D image (b) 3D volume.....	25
Figure 3.7	An object $f(x,y)$ and its projection $p(u, \theta)$ are shown for an angle θ (Kak and Slaney, 1999).	26
Figure 3.8	Coordinate system for projection and line integral.....	28
Figure 3.9	Illustration of matrix image in Back-projection.	30
Figure 3.10	Fourier transform theorem relates the Fourier transform of a projection to the Fourier transform of the object along a radial line.	33
Figure 3.11	Coordinate (u,v) and (x,y)	33
Figure 3.12	Filtered back-projection process.....	37
Figure 3.13	Filters in frequency domain.....	41
Figure 3.14	Filters in spatial domain.....	41
Figure 3.15	Illustration of a (a) equiangular and (b) equal-spaced sampling for fan beam	43
Figure 3.16	An equiangular fan beam geometry. Reconstructed pixel is expressed by (x,y) . Detector angle γ is the angle between the source-to-pixel line and iso-ray, Φ is the angle between x-axis and reconstructed pixel (x,y) (Kak dan Slaney, 1999).....	44

Figure 3.17	An equal-spaced fan. An equiangular fan beam geometry. Reconstructed pixel is expressed by (x,y) . Detector angle γ is the angle between the source-to-pixel line and iso-ray, Φ is the angle between x-axis and reconstructed pixel (x,y) and of s is the distance between iso-center and intersection of a ray with an imaginary detector line $D_1'D_2'$ (Kak dan Slaney, 1999).	46
Figure 3.18	Re-binning process (a) fan beam projections, and (b) individual rays in parallel beams.....	47
Figure 3.19	Example of ring artifacts in CT image.....	49
Figure 3.20	Flowchart to calculate the value of the Otsu threshold.....	54
Figure 4.1	Schematic block diagram of NMXCT setup	56
Figure 4.2	A photograph of NMXCT setup.....	57
Figure 4.3	Diagram of X-ray CT system. Detector has to be perpendicular to the rotational and source axis.....	58
Figure 4.4	General layout of multichannel ionization chamber. (a) signal strips , (b)anode electrode, (c) front-end electronics.	59
Figure 4.5	Toshiba X-ray tube	60
Figure 4.6	Rotation table for projections acquisition	61
Figure 4.7	Motion controller for rotation table	61
Figure 5.1	Main steps in XRecon for parallel data.....	65
Figure 5.2	Flowchart in XRecon for fan beam data	67
Figure 5.3	Solid cylindrical Perspex block of 50 mm	69
Figure 5.4	Solid cylindrical Perspex block of 120 mm	69
Figure 5.5	Cross section of first phantom.....	70
Figure 5.6	Cross section of second phantom.....	70
Figure 5.7	The beam profile of the detector output (a) normalized image without sample (b) corresponding line profile across the image.....	73
Figure 5.8	Sinogram for first phantom acquired at 80kV (a) 72 projections (b) 360 projections. The curve represents cable wire while the center rod is made of a material	74

Figure 5.9	Conversion process from fan beam sinogram to parallel sinogram (a) the original fan beam sinogram, (b) the mirrored fan beam sinogram in (a), (c) resulting parallel sinogram of the first fan beam sinogram, (d) resulting parallel sinogram of the mirrored fan beam sinogram, (e) the flipped parallel sinogram and (f) the second flipped parallel sonogram.....	76
Figure 5.10	COR for first phantom (a) summed image from projection at 0° and 360°, (b) line profile of summed image. The center line represents the number of pixel of the COR.	77
Figure 5.11	Sinogram for second phantom acquired at 80kV using 360 projections. The curve represents 3 plates were made of a material (aluminum)	78
Figure 5.12	Reconstructed image using first phantom (a) 72 projections, (b) 360 projections, (c) horizontal cross section along image a, (d) horizontal cross section along image b, (e) vertical cross section along image a, (f) vertical cross section along image b.....	79
Figure 5.13	Results for second phantom (a) reconstructed image using 360 projections (b) horizontal cross section and (c) vertical cross section.....	81
Figure 6.1	Photographic image of (a) agarwood tree, (b) agarwood trunk, (c) agarwood chips	85
Figure 6.2	Mass attenuation functions for different agarwood composites.....	87
Figure 6.3	Plot showing how attenuation coefficients vary according to X-ray energy for four different components.....	88
Figure 6.4	Simulated image represents wood cross section.....	89
Figure 6.5	The proposed quantification method.....	90
Figure 6.6	Photo of sample size	92
Figure 6.7	Flowchart for CT scanning.....	94
Figure 6.8	Resin in polyethylene tube with 1.90 mm diameter and 2 cm length	95
Figure 6.9	(a) CT image of resin before frozen, (b) CT image of resin after frozen, and (c) comparison of line profiles through the images.....	96

Figure 6.10	In cone beam geometry each fan is angled out of the source-detector plane of rotation. Vertical center is the optical axis.....	97
Figure 6.11	Oleoresin detection, (a) simulated wood CT image, (b) detected wood surface area, and (c) detected oleoresin regions.....	98
Figure 6.12	One of projected images from cone beam data	100
Figure 6.13	Reconstructed CT images with XRecon	105
Figure 6.14	Samples in group A (S1: Sample1, S2:Sample 2, S4: Sample 4, S8: Sample8), (a) CT image of agarwood, (b) total wood pixels, and (c) detected oleoresin pixels. Otsu threshold value in S1 (b), S2 (b), S4 (b) and S8 (b) are 0.35, 0.20, 0.23 and 0.19 respectively. Meanwhile a fixed threshold value of 168 is used in (c).....	113
Figure 6.15	Samples in group B (S3: Sample 3, S5: Sample 5, S7 : Sample 7), (a) CT image of agarwood, (b) detected total cross-section wood surface, and (c) detected oleoresin pixels. Otsu threshold value in S3 (b), S5 (b) and S7 (b) are 0.30, 0.23 and 0.23 respectively. Meanwhile a fixed threshold value of 168 is used in (c).....	115
Figure 6.16	Samples in group C (S9:Sample 9, S10:Sample 10), (a) CT image of agarwood, (b) detected total cross-section wood surface, and (c) detected oleoresin pixels. Otsu threshold value in S9 (b) and S10 (b) are 0.37 and 0.4118 respectively. Meanwhile a fixed threshold value of 168 is used in (c).....	116
Figure 6.17	Samples in group D(S6:Sample 6), (a) CT image of agarwood, (b) detected total cross-section wood surface, and (c) detected oleoresin area. Otsu threshold value in S6 (b) is 0.11. Meanwhile a fixed threshold value of 168 is used in (c).....	117
Figure 6.18	Oleoresin percentage in 2D CT image reconstructed using XRecon.	119

LIST OF SYMBOLS

		Page
I_o	Initial intensity	18
I	Intensity after attenuation	18
L	Thickness of object	18
μ	Linear attenuation coefficient	18
ρ	Density	19
μ/ρ	Mass attenuation coefficient	19
N	Number of projections	22
M	Geometric magnification	22
SOD	Distance between X-ray source and sample	22
SDD	Distance between X-ray source and detector	22
p	Projection	27
$p(\mu, \theta)$	Projection for constant θ	27
R	Radon Transform	29
$f_b(x, y)$	Back-projection image	31
$\frac{1}{r}$	Two-dimensional blurring function	32
$f(x, y)$	'density-function' of object	33
$P(\rho, \theta)$	Fourier transform of $p(u, \theta)$	33
$ \rho $	Filter in frequency response	37
$p'(u, \theta)$	Filtered operation with $ \rho $	37
$h(u)$	Filter in spatial domain	38
W	Highest frequency in Nyquist theorem	38
$H(\rho)$	Filter in frequency domain	38
$h(m)$	Filter in spatial domain	38
$R_\beta(\gamma)$	Equi-anglar fan projection	43

$R_{\beta}(s)$	Equal-spaced fan projection	44
β	The angle of the iso-ray formed with y axis	44
γ	The angle of the fan ray with iso-ray	44
Φ	Angle between x-axis and reconstructed pixel(x,y)	44
s	The distance between the iso-center and intersection ray	44
S_i	The source	44
D	Distance between the source S and the iso-center	44
D_1D_2	Detector line	44
D_1D_2'	Imaginary detector line	44
$\Delta\theta$	Angular increment between fan beam	47
$\Delta\gamma$	Angular interval used for sampling fan beam projection	47
T	Threshold value	52
$f(x, y)$	Object point	52
$h(x, y)$	Local property of pixel (x,y)	52
$g(x, y)$	Threshold image	52
ω_i	Weight of the class	52
σ_i	Variance of the class	52
μ_i	Mean of the class	55
COR	Center of rotation	72
nc_1	Number of column pixels in left sharp edge	72
nc_2	Number of column pixels in right sharp edge	72
$N_{oleoresin}$	Total pixels of oleoresin region	90
N_{total}	Total pixels of wood region	90
T_{total}	Global threshold	90
T_F	Fixed threshold	90

LIST OF ABBREVIATIONS

		Page
CT	Computedtomography	1
micro-CT	Micro-focus X-ray computed tomography	1
2D	Two dimensional	1
3D	Three dimensional	1
UGCT	University of Ghent Center of x-ray Tomography	7
BAM	Bundesanstalt für Materialforschung und - prüfung(Federal Institute for Materials Research and Testing)	7
UTCT	University of Texas the high-resolution x-ray Computed Tomography facility	7
CMOS	Complementary metal–oxide–semiconductor	7
CCD	Charge coupled device	7
nano-CT	Nano Computedtomography	8
BESSY	Berlin Electron Storage Ring Company for Synchrotron Radiation	8
ELETTRA	Enhanced Light Efficiency Cophasing Telescope Resolution Actuator	11
FBP	Filtered back-projection	11
PET	Positron Emission Tomography	17
ECT	Electrical Capacitance tomography	17
ERT	Electrical resistivity tomography	17
EIT	Electrical impedance tomography	17
SPECT	Single photon emission computed tomography	17
CST	Central slicetheorem	33
F	Fourier transform	33
F^{-1}	Inverse Fourier transform	33
HU	Housfield unit	53
XRecon	X-ray Reconstruction software developed in Malaysia Nuclear Agency	58
GUI	Graphical user interface	58
NMXCT	Nuclear Malaysia experimental X-ray CT setup	58

LDA	Linear detector array	58
MIC	Multichannel Ionization Chamber	61
ADC	Analog digital converter	61
NMB	North Minebea Motor Manufacturing Corporation	67
CITES	Convention on International Trade in Endangered Species	90
XCOM	X-ray photon Cross Sections database	91

LIST OF PUBLICATIONS

- Khair'iah Yazid, Bert Masschaele, Mat Rasol Bin Awang ,Mohd. Zaid Abdullah,Junita Mohamad Saleh,Abdul Aziz Mohamed,Mohd Ashhar Bin Hj Khalid. (2009) Three Dimensional Imaging Using Micro-computed tomography For Studying Gaharu Morphology: AIP Conference Proceedings - International Conference on Neutron & X-Ray Scattering "Neutron & X-Ray In Advanced Materials Research".29 June-1 July 2009. Kuala Lumpur,Malaysia. Vol. 1202:127-129.
- Khair'iah Yazid, Mohd. Zaid Abdullah, Junita Mohamad Saleh, Mat Rasol Awang(2009). Detection And Distribution Analysis Of Oleoresin In Gaharu Wood By X-ray Micro-computed Tomography(Micro-CT). Proceedings of the*Persidangan Kebangsaan Penilaian Ekonomi Sumber Hutan*, 11- 13 November 2009. Hotel best Western Premier Seri Pacific, Kuala Lumpur.
- Khair'iah Yazid (2009). An Experimental CT Setup with Linear Array Gas Detector: Practical Experiments As well As Image Reconstruction.Poster: Nuclear Malaysia Technical Convention 20096-8 October 2009.Malaysian Nuclear Agency
- Khair'iah Yazid,Mohd Ashhar Hj Khalid. Computer Implementation on X-ray Computed Tomography Image Reconstruction.Proceedings of International Conference on X-Rays and Related Techniques in Research and Industry. 29-30 November 2006. Palm Garden Hotel IOI Resort: Putrajaya.
- Khair'iah Yazid, Mohd Ashhar Hj Khalid(2006). Development of X-ray Computed Tomography (CT) System and Image Reconstruction. Poster: MINT R&D Seminar 2006.27-28 Jun 2006.Kuala Lumpur: Malaysian Institute Nuclear Technology Research.

KUANTIFIKASI OLEORESIN DI DALAM KAYU GAHARU MELALUI TOMOGRAFI MIKRO X-RAY BERKOMPUTER DAN PEMROSESAN IMEJ DIGITAL

ABSTRAK

Imbasan tomografi mikro x-ray berkomputer (CT) adalah teknik tanpa musnah yang terbukti berkesan untuk mengesan struktur dalaman kayu yang berskala kecil. Tesis ini dibahagikan kepada dua bahagian. Bahagian pertama melibatkan pengimejan semula dari unjuran tomografi mikro berkomputer. Satu program yang dinamakan XRecon telah dibangunkan untuk membolehkan pembinaan semula imej untuk sinaran selari dan sinaran kipas. Program ini dibuat berdasarkan kaedah unjuran balik bertapis. Satu setup eksperimen CT (NMXCT) telah dibina menggunakan sistem perubatan imbasan radiografi digital di Agensi Nuklear Malaysia. Tujuan adalah untuk membuktikan konsep sistem X-ray CT dan untuk mengesahkan program XRecon. Dua fantom dipilih untuk pengesahan program XRecon iaitu dua silinder blok Perspex padat. Keputusan menunjukkan XRecon sesuai digunakan untuk pembinaan semula imej CT dari unjuran sinaran kipas. Selain itu, sistem NMXCT menunjukkan kebolehan untuk mengesan objek dengan saiz minimum 2 mm. Didapati bahawa sistem NMXCT digunakan dalam kajian ini mungkin lebih sesuai untuk sampel yang lebih besar.

XRecon juga digunakan untuk pembinaan semula imej CT data mikro-CT. Oleh kerana mikro-CT data adalah sinaran kon, data unjuran paksi optik dipilih, yang diperoleh melalui geometri sinaran kipas, dan diubah menjadi data sinaran selari. Pembinaan semula imej CT tampak masuk akal tetapi terdapat beberapa artifak kelihatan pada imej. Keputusan menunjukkan XRecon mampu untuk membina semula imej unjuran paksi optik dari sinran kon. Masa yang dimabil untuk membina semula imej adalah kurang dari satu minit untuk 360 unjuran. Kualiti imej CT yang dibina

dengan XRecon dapat ditingkatkan dengan merancang fungsi penapis lebih tepat dan sesuai.

Bahagian kedua dari tesis ini bertujuan untuk mengukur jumlah oleoresin dalam imej CT gaharu menggunakan teknik pemprosesan imej. Pengesanan dan kuantifikasi *oleoresin* yang tepat sangat penting kerana nilai komersial gaharu berkaitan dengan kuantiti *oleoresin*. Untuk mengesan struktur-mikro *oleoresin*, sistem mikro-CT yang resolusi tinggi dan berkualiti tinggi amat diperlukan. Dalam tesis ini, sepuluh contoh kayu gaharu diimbas dengan sistem micro-CT desktop. Untuk pembinaan semula imej CT, XRecon telah digunakan. Didapati terdapat komponen dalaman imej CT gaharu mempunyai berbagai nilai bezajelas, yang kira-kira pemalar. Satu algorithm telah dibangunkan untuk mengekstrak and mengira jumlah oleoresin. Untuk mengekstrak maklumat oleoresin dari imej bina semula, imej CT harus ditukar menjadi gambar binari yang hanya mewakili oleoresin dan latar belakang kayu. Dua nilai ambang telah digunakan. Nilai ambang yang pertama digunakan untuk mengasingkan permukaan kayu dari latar belakang dan nilai ambang yang kedua digunakan untuk mengasingkan *oleoresin* dari kayu. Kaedah morfologi matematik digunakan untuk menghaluskan kawasan palsu pada imej binari. Peratus yang diperolehi dari oleoresin berkisar dari 0.7% hingga 0.001% dengan 0.001% ketidakpastian. Masa keseluruhan yang diambil dari proses pengimejan semula sehingga kuantifikasi adalah kurang dari 150 saat per imej dengan menggunakan komputer 2.0 GHz Pentium dengan 2.0 GB of RAM. Keputusan kuantifikasi yang diperolehi menunjukkan bahawa dengan kombinasi CT mikro dan teknik pengimejan berkomputer, oleoresin boleh diukur secara tepat.

QUANTIFICATION OF OLEORESIN IN AGARWOOD BY MEANS OF MICRO-COMPUTED TOMOGRAPHY AND DIGITAL IMAGE PROCESSING

ABSTRACT

Micro-focus X-ray computed tomography is a powerful non-destructive scanning technique to study internal micro-structure in wood. In this thesis, the study contains two parts. The first part involves the reconstruction of an image from CT projections. An algorithm referred to as XRecon program has been developed to allow slice reconstruction for parallel beam and fan beam data. The program was created based on filtered back-projection method. An experimental CT setup (NMXCT) was built by utilizing medical digital radiography scanning system in Malaysian Nuclear Agency. The objectives are to perform a proof-of-concept of X-ray CT system, and to validate the XRecon program. The target phantoms chosen for verification of the XRecon program were two solid cylindrical Perspex blocks. The results demonstrate that XRecon is suitable to reconstruct image from fan beam projections. In addition, NMXCT system showed the ability to detect objects with minimum size of 2mm. It was noticed that NMXCT system used in this study may have potential for imaging of bigger sample.

XRecon was also applied to scanned micro-CT data. Because of micro-CT consists of cone beam projections, the optical axis projection data was selected, which was acquired with fan beam geometry, and was converted to parallel beam data. The reconstruction looks reasonable, but some artifacts are visible in the image. The reconstruction time was observed to be less than a minute for 360 projections. The results show that XRecon is able to reconstruct vertical center from cone beam projections. The quality of reconstructed images using XRecon can be further improved by appropriately designing filter functions.

The second part of this thesis aims at quantifying oleoresin in agarwood CT image using image processing techniques. Auto detection and accurate quantification of oleoresin is particularly important, since the commercial value of agarwood is related to the present quantity of oleoresins. In order to detect the micro-structure of the oleoresin, high resolution of micro-CT system is required. In this thesis, ten agarwood chip samples were scanned with a desktop micro-CT system. The developed XRecon was applied in order to reconstruct the cross section CT image. It was observed that each component in the agarwood CT image has its own gray value, which is approximately constant. An algorithm was developed to detect and quantify the oleoresin. To extract the oleoresin information from the reconstruction, the image must be segmented into binary images that represent only oleoresin and wood background. Two threshold values were used. The first threshold value was used to separate the wood surface area from the background, while second threshold value was used to separate the oleoresin from the wood. Mathematical morphology operators were used for smoothing the spurious regions in the binary image. The obtained percentage of oleoresin ranged from 0.7% to 0.001% with 0.001% uncertainty. The overall processing speed from reconstruction to quantification takes a total time of about 150 seconds per image on a 2.0 GHz Pentium workstation with 2.0 GB of RAM. The quantification results show that with the combination of micro-CT and image processing, oleoresin can be accurately quantified

CHAPTER 1 INTRODUCTION

1.1 Introduction

Computed Tomography (CT) is one of non-destructive technique which allows visualization of the internal features of an object. CT produces images that correspond closely to the variation of X-ray attenuation within objects, which relates closely to density. Throughout the years, the resolution of X-ray CT systems has increased rapidly, in particular for micro-CT. Micro-CT is a miniaturized form of CT scanning, used to create 2D and 3D X-ray attenuation maps of specimens up to a few millimeters in size, with a resolution typically of the order of several microns (Buzug, 2008). The micro-CT X-ray system consists of a micro-focus X-ray tube and digital detector array. The latest digital detector array technology for industrial real-time digital imaging has a high dynamic range scale index ranging from 0 (black) to 4095 (white) for 12 bit or 65, 535 for 16bit images. This gray value range suits the need to evaluate both very dark and very bright regions in the same image. The smallest feature that a micro-CT system can detect depends on two factors: the detector's pixels and the minimum spot size of the X-ray source. As micro-CT are cone beam X-ray systems, three dimensional reconstruction methods are required to calculate the images (Wang et al, 1993). Micro-CT allows non-invasive mapping of 2D cross-sections of samples with micrometer resolution. Micro-CT scanning, combined with cone beam reconstruction, and followed by 3D volume-rendered reconstruction steps yield a virtual 3D volume image.

In recent years, micro-CT has increasingly been used effectively as a powerful tool for the detection and localization of internal features and for

analyzing morphological information in agricultural products. Additionally in some cases the features can be quantified from the CT image.

1.2 Problem Statement

One famous tropical forest product is agarwood. Agarwood is known as “The Gold Black Forest”, “Black Magic Wood” or “The Wood of the Gods”, and is one of the most valuable non-timber forest product (Wollenberg, 2001; Paoli et al., 2001).

The grading of agarwood is a complicated process (Barden et al., 2000). Agarwood can be grouped into different grades codes (Super A, A, B, C, D), which are determined based on the density of the resin and the type and intensity of the aroma it produces (Zich & Compton, 2001; Lim Teck and Noorainie, 2010). Traditionally, buyers often make the first determination of quality by using the water test, separating pieces that float (because of lower resin content) from those that sink (higher resin content, better quality). After they are dried, pieces are graded visually by human experts to identify the agarwood's grade, based on the amount of oleoresin on the wood surface. However, this technique is subject to bias and can be inaccurate. Visual assessment has led to several problems such as inconsistent grading results and is highly human expertise-dependent.

More recently, a prototype of an agarwood grade determination system using an image processing technique has been developed (Abdullah et al., 2007). In this technique, a digital camera system was used. Total of 74 images of agarwood were tested to obtain the grade. Image thresholding was employed to detect the percentage of the density of the black color by using grayscale images of agarwood as well as

determining the agarwood grade based on the density percentage. However, this prototype system is reported to be only suitable for lower grades of agarwood.

Conversely, non-destructive imaging provides an alternative method for grading agarwood. Auto detection and the accurate quantification of oleoresin is particularly important since the commercial value of agarwood is related to the quantity of oleoresins that are present.

To the best of the author's knowledge, tomographic technique has not been used in the agarwood industry. Non-destructive imaging can be used for improving the current conventional grading system and could lead to an improvement in the commercial value of agarwood. Investigating the amount of oleoresin in agarwood is great importance in terms of agarwood grading. Recent advances in micro-CT have increased the potential for detecting micro structures in wood, and a quantitative analysis can be made in 2D or 3D space. The results of this research might result in improving current conventional agarwood grading, and this could lead to an improvement in the commercial value of agarwood.

In this thesis, micro-CT was applied to detect oleoresin in agarwood, and then image processing was applied to the agarwood CT image to express the percentage of oleoresin inside the wood based on grayscale CT images of agarwood that could be the basis for the grading of agarwood.

1.3 Objective

The specific objectives of this study are:

- (1) To perform image reconstruction from CT projections.
- (2) To investigate the potential of micro-CT to detect oleoresin in agarwood.
- (3) To develop an image processing algorithm to detect and quantify oleoresin.

1.4 Scope of research

This study focuses on

- (1) Development of image reconstruction program for fan beam CT.
- (2) Development of fan beam data acquisition system to test the program.
- (3) Experimental work to validate the image reconstruction algorithm.

This study also covers

- (1) Experimental work to detect the oleoresin in agarwood using micro-CT system.
- (2) Development of an image processing technique to detect and quantify oleoresin in CT image.

1.5 Thesis Outline

Chapter 2 presents a literature review of micro-CT, the application of X-ray micro-CT in wood applications and the application of image processing in wood imaging. Chapter 3 focuses on the theory of CT and image reconstruction. Chapter 4 presents a description of the data acquisition system. Chapter 5 presents a description of the experimental work used to validate the reconstruction program developed in this study. Chapter 6 presents quantification of oleoresin in agarwood including a description of the samples used and the experimental works. It also includes the analysis and discussion of the results. The

conclusion to this thesis along with remarks and recommendations for future work, are presented in Chapter 7.

CHAPTER 2 LITERATURE SURVEY

2.1 Introduction

In many industrial fields, there is a strong interest in the understanding of the inner structure of objects or specimens. Advanced applications of materials need sophisticated measurement methods in terms of research, process development and quality control. X-ray micro-CT is a very powerful method for the non-destructive testing of materials. The great power of micro-CT lies in its ability to map 2D cross-sections of samples with micrometer resolution. In commonly used industrial CT-systems one X-ray tube is used (normally a 225 kV micro-focus tube or a 450 kV macro-focus tube) (Goebbels and Zscherpel, 2003; Simon et al, 2004). Compared with 2D parallel-beam and fan-beam CT, 3D cone-beam CT system is able to achieve a higher spatial resolution and a better utilization of photons (Wang et al, 1993).

2.2 Revolution and Recent Development in High Resolution CT Systems

X-ray CT scanners can be classified into four categories, based on their resolution and the size of objects that are most suitable for scanning. The four categories are summarized in Table 2.1.

Table 2.1 General classification of computed tomography(Ketcham & Carlson, 2001)

Type	Scale of observation	Scale of resolution
Conventional	m	mm
High-resolution	dm	100 μ m
Ultra-high resolution	cm	10 μ m
Micro-CT	mm	μ m

Micro-CT, which essentially comprises the design of the 3D CT, is typically used for non-destructive and three-dimensional microscopy associated with material testing and analysis. The two most crucial components of micro-CT are the X-ray tube and the two-dimensional detector array. CT with such high spatial resolution requires careful consideration of all factors which might influence the resolution, including the focal spot size of the X-ray tube, the influence of movements, vibrations and temperatures as well as the parameters of the detection system and even the reconstruction algorithm (Neuser and Suppes, 2007).

At present there are three leading research centers involved in the development of state of art high resolution micro-CT systems. First is Center of X-ray Tomography at the Ghent University (UGCT) in Belgium. The second is the Federal Institute for Materials Research and Testing (BAM) in Germany and the third is University of Texas High Resolution X-ray CT facility (UTCT) in USA. These top research centers have set up their own high resolution CT systems and have developed powerful reconstruction software.

UGCT has developed several multidisciplinary micro-CT scanners up to 160 keV (Masschaele et al, 2007). The main advantage of these scanners is their flexible set-up that different detectors can be used to optimize the scanning condition. A variety of detectors are available at this center, including large array detector scanner utilizing flat-panel amorphous silicon arrays (VARIAN Paxscan 2520V), cooled CCD detector with thin scintillator in camera box (Photonic Science VHR) and several remote flat panel CMOS detectors (Rad-Icon CMOS RadEyeHR.). Beside this variety of detectors, UGCT has closed and open type micro-focus tube (Feinfocus FXE-160.50). The last type allows

one to replace filaments and targets, but is more expensive than the closed type. For high energy applications, UGCT has an electron accelerator up to 15MeV energy that can be used for scanning large dense objects. The highest spatial resolution of micro-CT in UGCT is 2 μm (Masschaele et al, 2007). UGCT has also developed a state of art nano-CT scanner that utilizes a dual head transmission X-ray tube. The dual head means that there are two tube heads, a high power directional head and a nano transmission head. The highest possible image resolution is equal to the size of the X-ray spot (900 nm at 40 kV) (Masschaele et al, 2007; Dierick et al., 2008). Beside state of art micro-CT and nano-CT systems, UGCT has developed in-house software for scanner control, sample reconstruction, analysis and visualization. UGCT has successfully commercialized their reconstruction software package Octopus (Dierick et al., 2004; Vlassenbroeck et al., 2007). Additionally, UGCT provides a wide range of application from biological to geological samples and from cultural heritage to industrial objects.

The Federal Institute for Materials Research and Testing (BAM) CT Working Group has developed several high resolution CT scanners using different kinds of micro focus X-ray tubes for laboratory use and has a sub-micron CT facility at Berlin Electron Storage Ring Company for Synchrotron Radiation (BESSY). The applications in BAM CT cover a broad spectrum analyzing the structure and assembly of rare small insects, characterizing fiber reinforced material, metal matrix composites up to the dimensional analysis of casting and flaws in welding seams (Goebbels et al, 2003). There are four Industrial CT scanners with X-ray sources with energy between 10 keV and 12MeV which can be used for many applications. In order to extend the applicability of micro-CT, a novel micro-CT scanner has been developed in house for large and dense object

applications. This novel 3D-CT scanner that was set up at BAM, consists of a bipolar 320kV micro-focus tube and a flat panel detector of amorphous silicon. The scanner is suitable for scanning objects of between 1 and 30 cm diameter. For sub-micrometer range measurements, the BAM CT Group has a high resolution synchrotron-based micro-CT using a hard X-ray BAMsynchrotronline at BESSY. The monochromatic synchrotron light between 8 keV and 80 keV is attained through the use of a fully automated double multilayer monochromator (Bakker, 1999). A monochromator is an optical device that mechanically selects narrow bands of wavelengths of light or other radiation chosen from a wider range of wavelengths. The sub-micron system allows the imaging of a micro-structured object as well as multi-component specimens which can be performed with different contrast modes and resolutions. The highest possible image resolution is up to 1.0 μm (Rack et al., 2008). The system can be used for absorption and refraction, as well as phase contrast.

The UTCT Facility has several unique high resolution CT systems for applications in geosciences and in biological and engineering sciences. High resolution CT systems at UTCT utilize a dual-spot 420kV X-ray source (Pantak HF420) for large specimens, and a 200 kV tube for ultra-high resolution work (Feinfocus FXE-200.20). The great flexibility of the ultra-high resolution system allows the imaging of specimens from several cm to a few mm in diameter, with a spatial resolution from $\sim 250 \mu\text{m}$ to $\sim 5 \mu\text{m}$ (Ketcham and Carlson, 2001). UTCT also has a micro-CT scanner with the capability of scanning specimens which are smaller and less attenuating. The micro-CT scanner features a Hamamatsu X-ray source capable of energies from between 40 keV and 150 keV. The detectors are mounted on microscope objectives with magnifications ranging from 0.5X to 40X; the former yields a field of view of $\sim 30 \text{ mm}$, whereas the

latter yields ~ 0.65 μm . The spatial resolution for the micro-CT scanner ranges from 30 μm to less than 1 μm . This micro-CT scanner also offers the advantage of enhanced phase contrast in such a way as to better image materials with low mean atomic numbers such as soft tissues and polymers.

It can be concluded that micro-CT and nano-CT technology is improving rapidly with the production of compact X-ray tubes with a focal spot of up to several microns in size and the latest digital detector array technology. Micro-CT performance strongly depends on the characteristics of the X-ray source. The X-ray source with focal spot of size up to several microns allows to obtain radiographs of a small specimen with a large geometrical magnification and, consequently, to achieve a very high spatial resolution. The high spatial resolutions of the micro-CT and nano-CT make it well suited for imaging small samples.

2.3 Application of micro-CT

Micro-CT is a novel technology ideally suited to wide range of applications. The application areas include composites materials, carbon-based materials, paper and wood microstructure, biomedical applications, industrial components, etc.

For small sample application, micro-CT has been applied to detect microdiamonds in kimberlite cores and to characterize the X-ray attenuation properties of the kimberlite (Schena et al., 2005). Synchrotron radiation at multipurpose synchrotron facility ELETTRA in Italy was used. The experiments were carried out at energy range was between 8 keV and 35 keV. CT image reconstructed with filtered back-projection (FBP) algorithm from 720 projections around 180° . Another experiment was

tested with a commercial micro-CT system with operating condition 90kV, 0.6 mA, single image frame, exposure time 2 seconds and 720 projections. The spatial resolution is 25 μ m. The result shows the microdiamonds clearly seen as black spots due to the lower attenuation compared to kimberlite cores.

As micro-CT is non-destructive tool, micro-CT scans allow comparison of images and data of samples before and after treatment. Because of this ability, micro-CT has been successfully applied for stone characterization in historical buildings (Castele et al, 2007). They employed a desktop micro-CT to investigate morphological parameters such as total porosity and the pore size distribution. The samples were cut to 3 x 3 x 3 mm³ and the investigations were carried out before and after treatment. During projections acquisition, camera binning was applied; using 2 x 2 pixels on the detector row and pixel resolution of 2.5 μ m was obtained suitable for the size of the samples. A frame averaging of 4 and rotation step of 0.4° over 180° were chosen to minimize the noise. After reconstruction process, a global thresholding was performed to create binary images of porosity. The experiment result shown that total porosity can be determined before and after treatments using micro-CT.

Furthermore, micro-CT has been tested to analyze morphology and composition exemplified at porous asphalt (Goebbels et al., 2007). The study utilized micro-CT system at BAM for large and dense samples. The investigations were performed with high voltage of 140 kV and current of 160 μ A. The beam hardening filtering was applied with 0.25 mm Cu and 0.5 mm Ag. The integration time per projection was 6 seconds. The number of projections was 900 for full rotation of 360°. They found that

micro-CT can be used as accurate non-destructive tool to determine morphology of open or closed porosity in multi component porous asphalt.

The above studies indicate that application of micro-CT for imaging internal object in small sample is reliable and has a great potential. Micro-CT is currently a well-established imaging methodology that can be used to distinguish internal structural features. It has been widely used in several material science disciplines.

2.4 Application of micro-CT in wood research

X-ray CT has become an important inspection tool with regards to defects in wood. However, the spatial resolution in conventional CT is usually not sufficient to investigate the wood structure at the cellular level (Trtik et al., 2007).

In recent years, micro-CT has been successfully applied to wood research and has been used to determine the anatomical characteristics and morphological information of wood (Steppe et al., 2004). Two samples were used in this study. Image processing techniques were applied to determine the inner vessel diameters, the transverse cross-sectional surface area of the vessels, the vessel density and the porosity. The visual inspection of the micro-CT images on hardwoods has revealed very good correspondence and has provided information on vessel diameter, vessel area, vessel density, and porosity with the same accuracy as classical optical micrographs.

Micro-CT was used as a detection tool for localization of certain product inside wood (De Vetter et al., 2006). They used desktop micro-CT system with spatial resolution of 10 μm . The wood samples were scanned at 130 kV, current at 76 μA and

exposure time of 2.3 m. Multiple-frame averaging and rotation step of 0.4° were chosen to minimize the noise in images. Another experiment was carried out using scanning electron microscopy to view the anatomical structure of wood. They found that scanning electron microscopy and micro-CT are complementary and can offer important information concerning the localization of certain compounds inside wood.

These researchers have concluded that the use of desktop micro-CT in wood research offers an interesting potential for all those who need qualitative as well as quantitative data with regard to wood anatomical characteristics in either 2D or 3D space, in a short period of time.

Furthermore, other micro-CT applications for wood research have been tested and evaluated using synchrotron radiation (Forsberg et al., 2008; Trtik et al., 2007). A summary will be given here. An analysis of infested coated wood has been explored with X-ray sub-micron CT (Van den Bulcke et al., 2008). Sub micro-CT for wood imaging with a resolution of less $1\ \mu\text{m}$ gives good result up to cell wall level (Trtik et al., 2007). In-situ experiments using synchrotron radiation micro-CT has shown potential for observing structural changes in wood specimens (Forsberg et al., 2008). More recently available imaging technique called phase-contrast micro-CT, has shown potential for capturing the 3D microstructure of wood with high spatial resolution $0.5\text{--}1\ \mu\text{m}$ using synchrotron sub micro-CT (Mannes et al., 2010). The combination of phase-contrast technique and synchrotron radiation has been used to determine the characteristics of the shrinkage behavior of Norway spruce wood at the cellular scale (Derome et al., 2010). Synchrotron micro-CT has been successfully used to characterize wood degraded by decay fungi (Illman and Dowd, 1999). The above

studies indicate that wood research in sub-micronscales has large potential and highly demand.

2.5 Image processing in wood imaging

Image processing is a vital part in the automatic detection and classification of wood images. Once a digital image has been acquired, there are many mathematical algorithms that can be used to detect and classify the features of interest. Several studies have been carried out to develop fully automatic detection of the internal features in cross-section CT images of wood. The majority of imaging applications to wood have been based on segmentation algorithms. Most researchers have used various segmentation techniques to investigate the extraction of features in images of wood. Other features of detection techniques in wood images include edge detection, region extraction and colour segmentation (Funck et al., 2003).

A grayscale histogram-based thresholding technique has been used to detect cracks in cross-sectional CT images of logs (Bhandarkar et al., 1999). The method exploits the fact that a crack in the wood is composed of a void volume of air. Due to air being of a lower material density than wood, the pixels in the CT image that represent cracks have a much lower grayscale value than other pixels.

Improvement for the existing defect-detection system was continued using morphological operation techniques (Sarigul et al., 2003). The study employed several binary morphology operations in binary images to smooth the boundaries of the detected regions. The objective is to classify knot, split, bark, and clear wood in CT

image of log. This technique has shown impressive visual results and good results for the classification in post-processing step.

In addition to automatic detection in CT images of wood, edge detection was employed to detect pith in CT image of spruce log (Longuetaud et al., 2004). A combination of Sobel edge operators and Hough transform was applied to detect the pith in the CT image. Total of 18,700 slices of CT images was used in order to develop an automatic detection of the pith.

CHAPTER 3 THEORY

3.1 Introduction

“Tomos” is the Greek word for “cut” or “section” meaning representation. Thus, tomography means imaging a very small section such as a thin slice that uses a source (e.g. X-ray, ultra-sound, microwave, etc.) to examine an object. As the term is used today, Computed Tomography (CT) is also known as Computerized Tomography or Computer Aided Tomography or Reconstructive Tomography, and is a well-known non-invasive imaging technique that allows for complete visualizing of the internal structure of an object without superimposition. Tomography works by creating digital radiography images at different angles (projections). With the aid of a computer, these projection data can be joined together to reveal the details of the internal structure of the object.

While X-ray CT may be the most familiar application of tomography, tomography can be performed using other imaging modalities, including ultrasound, magnetic resonance, nuclear-medicine, and electrical techniques. Table 3.1 explains each tomography modality. Each tomography modality measures different properties of an object.

Since the development of X-ray CT by Housfield in 1972, the basic principle has not changed. Transmission X-ray CT is conceptually simple, in that an object is placed between an X-ray source and a detector, and the object is rotated while the X-ray is passed through it, collecting the information about its internal structure. As the object rotates from 0° to 360° in small angular steps around the beam, it creates hundreds of

planar radiograph images called projections. For each projection, an intensity map representing an attenuation profile of the scanned object is recorded by a detector plane. Measured projections are manipulated by a computer according to a reconstruction algorithm, to produce a two-dimensional map of the attenuation coefficients in the irradiated cross section. The objective of CT image reconstruction is to determine how much attenuation of the narrow x-ray beam occurs in each volume pixel (voxel) of the reconstruction matrix. In the case of X-ray tomography, the gray levels in a CT slice image correspond to an X-ray attenuation coefficient. X-ray attenuation is primarily a function of X-ray energy, and of the density and composition of the material being imaged.

Table 3.1 Comparison between different tomography modalities

Tomography	Working Principle	Image reconstruction
Transmission Tomography (X-ray)	The number of X-ray photon transmitted through object along individual projection	The distribution of linear attenuation in the slice being imaged
Positron Emission Tomography (PET) (nuclear medicine)	The number of photons emitted from object along individual projection	The distribution of radiotracer concentration administered to the patient in the slice being imaged
Diffraction (ultrasound)	The amplitude and phase of scattered waves along a particular line between source and detector	The distribution of refractive index in the slice being imaged
Electrical Tomography ECT: Electrical capacitance tomography, ERT: Electrical resistivity tomography, EIT: Electrical impedance tomography	Exploit differences in the electrical properties of different materials	The distribution of the content of an object in terms of electrical resistivity, capacitances, and inductance changes

When a narrow beam of mono-energetic photons such as X-rays penetrate the surface of a material, it experiences a change in its intensity, owing to the absorption or

scattering that occurs during the travel of the beam across the material (Lambert–Beer law). The Lambert–Beer law can be expressed as follows:

$$I = I_0 e^{-\mu L} \tag{3.1}$$

An attenuation intensity diagram is shown in Figure 3.1

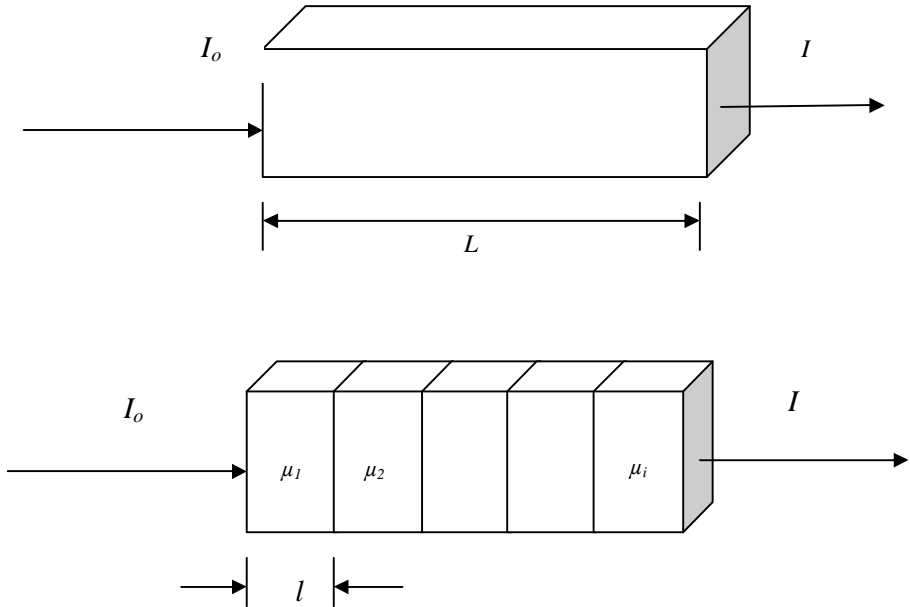


Figure 3.1 Attenuation diagram of Beer law

In the case of the object is heterogeneous, Equation (3.1) can be expressed as follows:

$$I = I_0 e^{-\mu_1 \Delta l} e^{-\mu_2 \Delta l} e^{-\mu_3 \Delta l} e^{-\mu_4 \Delta l} e^{-\mu_5 \Delta l} \dots e^{-\mu_n \Delta l} = I_0 e^{-\sum_{n=1}^N \mu_n \Delta l} \tag{3.2}$$

where I_0 is the initial intensity of X-ray, I is the X-ray intensity after attenuation, Δl is the thickness of the detected object, and μ_n is the attenuation coefficient of different object (Kak and Slaney, 1999). The coefficient μ must have the dimension of length^{-1} . It is called the linear attenuation coefficient. It is generally expressed in cm^{-1} . In general, μ

changes with X-ray energy and varies with selection of material. From Equation (3.2), it is clear that object with higher μ are more attenuating to X-ray photons than objects with lower values. The linear attenuation coefficient depends on the thickness of the material, density of the material, atomic number and photon energy (Amersham Health, 2003).

Usually, the dependency of the linear attenuation on the density of the material is overcome by normalizing it to the density. The normalized value of the linear attenuation is called the mass attenuation (μ/ρ). It is usually expressed in units of cm^2/g . Therefore Equation (3.1) can be expressed as follows:

$$\frac{I}{I_0} = e^{-\left(\frac{\mu}{\rho}\right)\rho L} \quad (3.3)$$

where (μ/ρ) is mass attenuation coefficient of a given material, ρ is the density of the given material and L is the thickness of the material. It can be concluded that mass attenuation coefficient is a basic used in the calculation of penetration.

3.2 Type of CT systems

In most cases, there are three types of CT systems for industrial applications. Different configurations of CT system can be optimized for imaging objects of various sizes and compositions. Currently, the selection of CT system geometry is application specific. The geometry for fan beam, cone beam and parallel beam are shown in Figure 3.2. Details description about fan beam system, cone beam system and parallel beam system are summarized in Table 3.2.

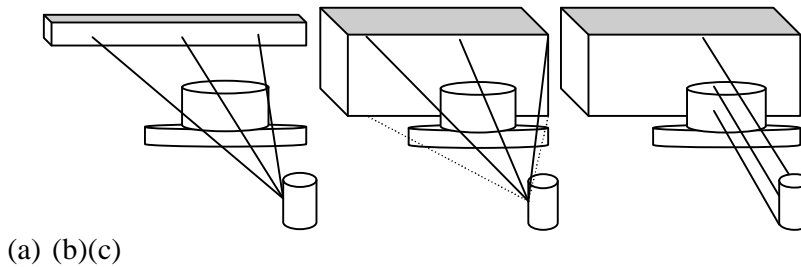


Figure 3.2 Geometry for each CT system (a) fan beam, (b) cone beam and (c)parallel beam

Table 3.2 Descriptions of each CT system geometry

Tomography geometry	Descriptions
Fan Beam	<ul style="list-style-type: none"> ▪ Source: X-ray point ▪ Consisted of a collimated fan beam ▪ The detector has linear array ▪ Time consuming to cover a volume ▪ Scanning full rotation 360^0
Cone Beam	<ul style="list-style-type: none"> ▪ Source: X-ray point ▪ Multiple fan beam planes are collected simultaneously to cover a volume. ▪ X-ray source ▪ The detector has planar shape. ▪ Shorter data acquisition time ▪ Scanning rotation: 360^0
Parallel Beam	<ul style="list-style-type: none"> ▪ Source: Synchrotron ▪ Set of parallel rays projection ▪ The detector has planar shape ▪ Scanning rotation :180^0

3.3 Image Reconstruction

A crucial step in CT is the calculation of the image from the acquired data set of projections. The mathematical methods are of central importance in the new technologies of radiographic and radiosopic image reconstruction (Brooks and Di Chiro, 1976).The equations governing image reconstruction were first solved in 1917 by Radon, who was concerned with applications in gravitational theory. Cormack (1963,1964)introduced Fourier transforms to reconstruction algorithm, where in that he

derived the mass distribution inside an object from its radiographic projection images taken from different projection images. Later in 1980, Herman introduced filtered back-projection to reconstruction algorithm (Herman, 1980). The filtered back-projection is the most popular reconstruction. For easily understanding of the basic principle of two dimensional CT reconstructions, this chapter will discuss the definition of line integral, projection and sampling geometry.

The objective of image reconstruction is to determine how much attenuation of the narrow beam occurs in each volume pixel (voxel) of the reconstruction matrix. For CT, it is the linear attenuation of the object. In this chapter, reconstructions for cross-section 2D images will be focused. Fundamentally, transmission tomographic imaging deals with reconstructing an image from its projections. Projections data in its simplest terms are a set of measurements over of range of angular orientation around the object. Each measurement represents the summation or line integral of attenuation coefficient of an object along a particular ray path (Kak and Slaney, 1999). First set of measurements along paths that are parallel to each other and are uniformly spaced, as shown as solid lines as shown in Figure 3.3 This measurement forms a “view” or “projection”. The measurement process is repeated at different angle, as shown in the dotted line in Figure 3.3. This process continues throughout full rotation (360 degree). During the entire process, the angular increment between adjacent views remains constant and the scanned object remains stationary at the same location. These projection data are used to create two dimensional images that are called a CT slice because they correspond to what would be seen if the object was sliced along the scan plane.

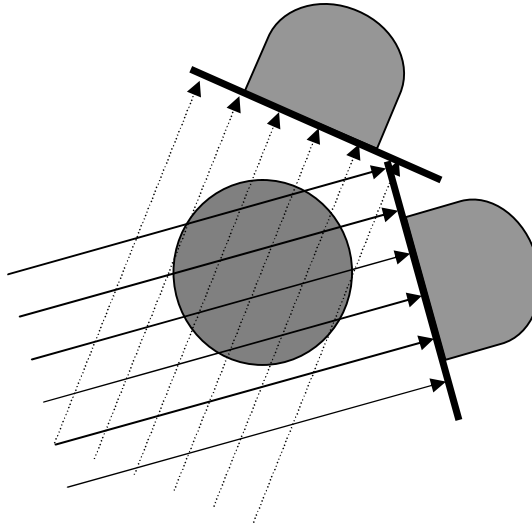


Figure 3.3 Data sampling pattern.

3.4 Projection geometry and system geometry

The sampling geometry depends on the CT system geometry (see Figure 3.4). Parallel beam geometry requires projection images with equi-angular separation between 0° and 180° . Fan and cone beam geometry require projections over 360° . A data set with N samples per projection and $1.5 \times N$ projections produces an image with $N \times N$ pixels (Barret and Swindel, 1981).

Geometric magnification technique is used to improve spatial resolution in CT image. In CT, the geometric magnification M can be calculated as follows:

$$M = \frac{SDD}{SOD} \quad (3.4)$$

where SDD is ratio of the distance between X-ray tube focal point and the system detector and SOD is the distance between the X-ray tube focal spot and the sample. $M=1$ means that the object is close to the source. SDD and SOD are illustrated in Figure 3.5.

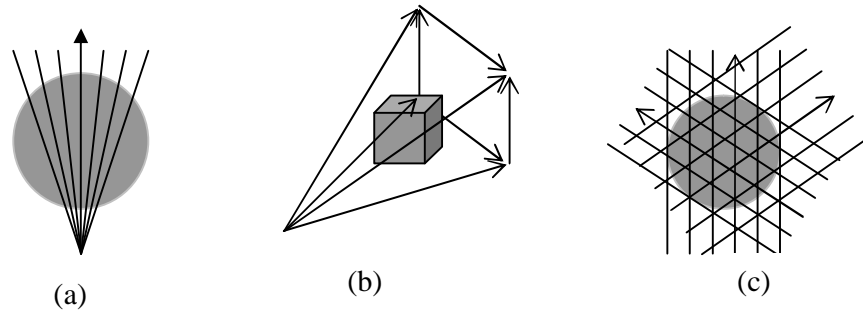


Figure 3.4 Projection geometry for each CT system (a) fan beam projection, (b) cone beam projection and (c) parallel beam projection

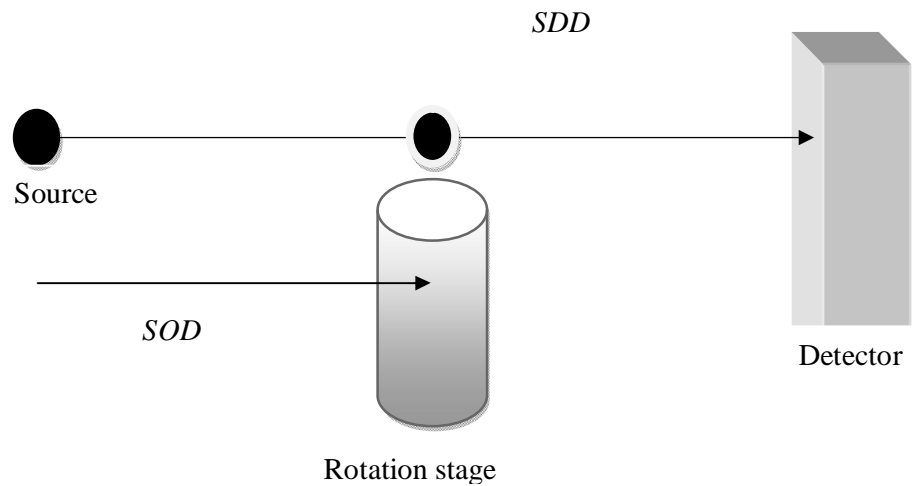


Figure 3.5 Illustration of distance between X-ray tube focal point and the system detector (SDD) over the (distance between the X-ray tube focal spot and the sample (SOD) in CT system

The closer the sample can get to the X-ray tube focal spot the greater the geometric magnification a system can achieve. As a result, the thinnest samples will always be able to achieve the highest geometric magnifications in a CT system. The X-ray tube focal spot is the position within the tube where the X-rays are actually produced and not the same place as the outer cover of the tube.

In CT, spatial resolution is defined by the size of the imaging voxels. A voxel is the volume element, defined in 3D space. Its dimensions are given by the pixel, together with the thickness of the slice. A pixel is a picture element that represents the smallest sampled 2D element in an image. Pixel size is the size of the detector pixel. A comparison between pixel and voxel is shown in Figure 3.6. In CT, voxel size can be calculated as follows:

$$Voxelsize = \frac{Pixelsize}{M} \quad (3.5)$$

where M is the object magnification.

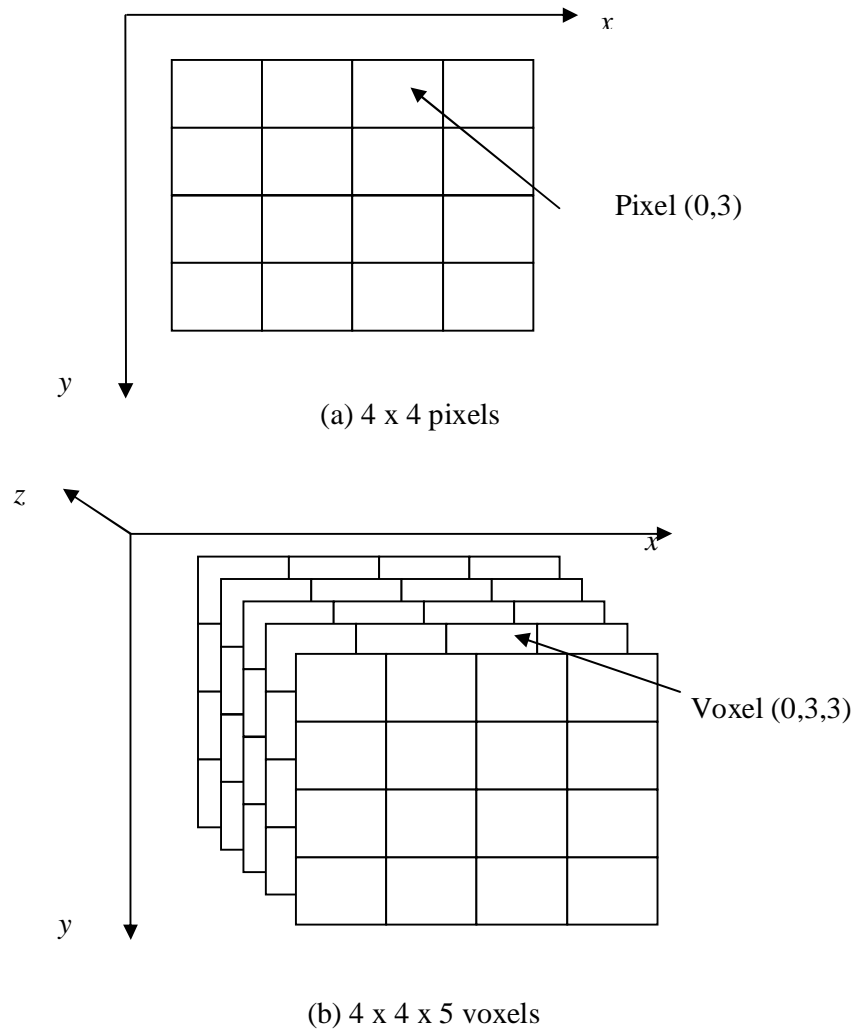


Figure 3.6 Comparison pixel versus voxel (a) 2D image (b) 3D volume

3.5 Projection and line integral

Referring to Lambert-Beers law (Equation 3.1), a line integral, as the name implies, represents the integral of some parameter of the object along a line